



Rational design of agonists for bitter taste receptor TAS2R14: from modeling to bench and back

Antonella Di Pizio^{1,2} · Lukas A. W. Waterloo³ · Regine Brox^{3,4} · Stefan Löber³ · Dorothee Weikert³ · Maik Behrens⁵ · Peter Gmeiner³ · Masha Y. Niv¹

Received: 8 February 2019 / Revised: 11 June 2019 / Accepted: 14 June 2019
© Springer Nature Switzerland AG 2019

Abstract

Human bitter taste receptors (TAS2Rs) are a subfamily of 25 G protein-coupled receptors that mediate bitter taste perception. TAS2R14 is the most broadly tuned bitter taste receptor, recognizing a range of chemically diverse agonists with micromolar-range potency. The receptor is expressed in several extra-oral tissues and is suggested to have physiological roles related to innate immune responses, male fertility, and cancer. Higher potency ligands are needed to investigate TAS2R14 function and to modulate it for future clinical applications. Here, a structure-based modeling approach is described for the design of TAS2R14 agonists beginning from flufenamic acid, an approved non-steroidal anti-inflammatory analgesic that activates TAS2R14 at sub-micromolar concentrations. Structure-based molecular modeling was integrated with experimental data to design new TAS2R14 agonists. Subsequent chemical synthesis and in vitro profiling resulted in new TAS2R14 agonists with improved potency compared to the lead. The integrated approach provides a validated and refined structural model of ligand–TAS2R14 interactions and a general framework for structure-based discovery in the absence of closely related experimental structures.

Keywords Bitter taste receptor · GPCRs · Drug design · Structure-based modeling · Bioisosteric replacement

Electronic supplementary material The online version of this article (<https://doi.org/10.1007/s00018-019-03194-2>) contains supplementary material, which is available to authorized users.

✉ Maik Behrens
m.behrens.leibniz-lsb@tum.de

✉ Peter Gmeiner
peter.gmeiner@fau.de

✉ Masha Y. Niv
masha.niv@mail.huji.ac.il
<https://biochem-food-nutrition.agri.huji.ac.il/mashaniv>

¹ The Robert H. Smith Faculty of Agriculture, Food and Environment, Institute of Biochemistry, Food Science and Nutrition, The Hebrew University, Rehovot, Israel

² Section In Silico Biology & Machine Learning, Leibniz-Institute for Food Systems Biology at the Technical University of Munich, 85354 Freising, Germany

³ Department of Chemistry and Pharmacy, Friedrich-Alexander-University Erlangen-Nürnberg, Erlangen, Germany

⁴ Department of Transfusion Medicine and Haemostaseology, University Hospital, Erlangen, Germany

⁵ Section Chemoreception and Biosignals, Leibniz-Institute for Food Systems Biology at the Technical University of Munich, 85354 Freising, Germany

Introduction

G protein-coupled receptors (GPCRs) are seven-transmembrane proteins that are involved in signal transduction across the cell membrane. Due to their remarkable role in mammalian physiology, GPCRs and their ligands are among the most active research areas in academia and pharmaceutical industry [1, 2]. Human senses, such as vision, olfaction, and some of the taste modalities, are mediated by GPCRs [3, 4]. Sweet and umami molecules are recognized by TAS1Rs, belonging to class C GPCRs [5]. In contrast, bitter substances interact with TAS2Rs, which are grouped as a subfamily of class A GPCRs based on their ligand-binding pocket localization [6]. In humans, there are 25 TAS2R members, representing about 4% of all GPCRs [7]. Bitter taste receptors were recently shown to be expressed extra-orally [8] and their diverse physiological roles are under current study [9–13]. Bitter taste strongly influences food acceptance [14] and drug compliance [15]. Thus, TAS2R antagonists may serve for bitter taste masking, in particular for pediatric drugs, while TAS2R agonists may be relevant for therapeutic applications [16, 17].

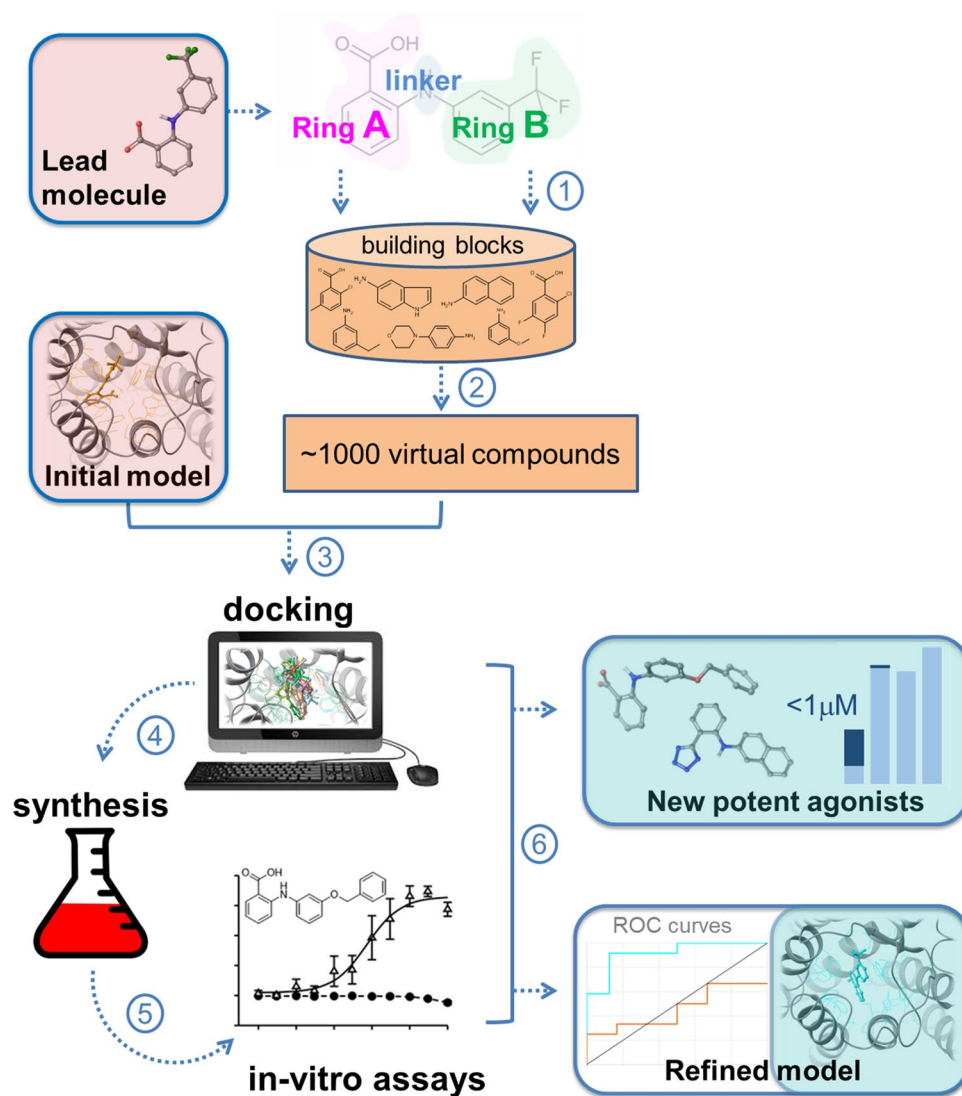
Recent breakthroughs in the structural determination of GPCRs have greatly advanced our understanding of GPCR signaling [18]. Structural knowledge facilitates integrative approaches including structure-based modeling, chemical synthesis, and biological hit evaluation for the discovery of promising new lead compounds [19, 20]. Despite the dominant share of taste and smell receptors in the human GPCR-ome, no experimental structure is yet available. Iterative modeling of TAS2Rs has been successfully applied to define the agonist-bound conformation of bitter taste receptors and to discover ligands among known drugs and commercially available molecule libraries [21–27]. However, to the best of our knowledge, this is the first example of rational design and synthesis of ligands for bitter taste receptors.

TAS2R14 is an interesting target both physiologically and structurally. It was shown to mediate nitric oxide-driven

endogenous innate immune responses and suggested as a target for treating airway infections [11, 28] and to be expressed in the testis and in spermatozoa, with possible implications for male fertility [29]. As an additional evidence of connection between bitter taste and physiological functions, TAS2R14 ligands are common among approved drugs [27, 30] and traditional Chinese medicines [31]. In terms of structure and receptive range, TAS2R14 orthosteric-binding site can accommodate multiple dissimilar molecules [8, 32, 33], and even large modifications of known agonists can be tolerated by the receptor [34].

The interdisciplinary approach in the current work integrates homology modeling and docking with chemical synthesis and *in vitro* pharmacological characterization and enables rational design of TAS2R ligands, as schematically presented in Fig. 1.

Fig. 1 TAS2R14 agonist design strategy. Workflow outlining the process of computational design of flufenamic acid analogs (1–3), synthesis of selected compounds and bioisosteres (4), functional assays (5), and analysis of experimental results and TAS2R14 model refinement (6)



Results

Structure-based analyses combined with extensive mutagenesis data have previously allowed us to propose a binding mode of flufenamic acid to TAS2R14, in which the ligand was found to form H-bond interactions with Asn93^{3.36} and Trp89^{3.32} (superscripts indicate Ballesteros–Weinstein numbering [35]) and π – π -stacking interactions with Trp89^{3.32}, Phe186^{5.46}, and Phe247^{6.55} of TAS2R14 [36], revealing an unoccupied region of the binding pocket (Fig. S1). In the current work, we hypothesized that flufenamic acid derivatives can establish additional contact points in this region, leading to stronger affinity. A docking screen was performed to identify suitable candidates, starting from the initial model from a previous study [36] (provided as Supporting Information, initial_model_TAS2R14.pdb). A virtual combinatorial library of ~1000 compounds was generated by linking commercially available building blocks (ring A and ring B surrogates) in a one-step chemical reaction (Fig. 1, steps 1 and 2). This library was docked to the TAS2R14 initial model (Fig. 1, step 3). Top scoring compounds were visually inspected and 11 compounds (**10–18**, **20** and **22**) were selected for chemical synthesis (Fig. 1, step 4).

In addition, two popular medicinal chemistry concepts were applied, namely bioisosteric replacement [37] and conformational restriction [38], to design additional flufenamic acid analogs. Thus, the carboxylic acid was replaced by either a tetrazole or a sulfonamide moiety, leading to compounds **28–34**. These bioisosteres should be able to maintain the H-bond interaction with Asn93^{3.36}, while allowing the exploration of different chemotypes. Moreover, they have the potential to improve the bioavailability for extra-oral TAS2R14 targeting [37].

The response of TAS2R14 to the flufenamic acid derivatives was investigated in a calcium-imaging assay using HEK293T cells expressing the chimeric G protein $G\alpha_{16\text{gust}44}$ (Fig. 1, step 5) [39, 40]. Out of the 19 synthesized ligands, 12 activated TAS2R14 with EC₅₀ concentrations below 1 μM , with three of them being more potent than the lead structure flufenamic acid (EC₅₀ 238 nM), see Table 1 for EC₅₀ and SEM data and Fig. S2 for dose–response graphs. Replacement of the *meta*-positioned-CF₃ substituent on ring B of flufenamic acid with an ethyl- or aminophenyl group (**10** and **12**) resulted in reduced activity (EC₅₀ 993 nM and 846 nM) and even the bulky benzyloxy-substituent (**15** and **16**) was well tolerated (EC₅₀ 516 nM and 896 nM). The addition of a second *meta*-positioned –CF₃ group to ring B (**11**) increased the potency even further (EC₅₀ 117 nM). A comparison of the carboxylic acids **12–14** clearly demonstrates that an *ortho*-substitution on ring B is not tolerated, as a dramatic loss of activity was measured for **13** and **14**. In contrast, ligands **17** and **29** with an enlarged 2-naphthalene

system instead of phenyl ring B still caused substantial TAS2R14 activation. However, the naphthalene substitution in ring B combined with fluorine substituents to ring A caused a loss of activation in compound **18**. Compounds **14**, **16**, and **18** demonstrate that an introduction of fluorine substituents to ring A does not significantly change EC₅₀ compared to the respective unsubstituted derivatives **13**, **15**, and **17**. A substantial decrease or even complete abolishment of TAS2R14 activity was observed when the amine linker was modified by insertion of a methylene unit (**20**) or replaced with an ether linker (**22**).

Bioisosteric replacement of the carboxylic acid with a sulfonamide resulted in a complete loss of TAS2R14 activation for **33** and **34**. On the contrary, substantial TAS2R14 activation was detected for the 5-substituted tetrazoles **28–32**. Importantly, tetrazoles **31** and **32** comprising one or two trifluoromethyl-substituents on ring B belong to the most potent ligands of the series (EC₅₀ 171 nM and 117 nM). Conformational restriction resulting in the tricyclic flufenamic acid derivative **38** caused abolishment of TAS2R14 activity, indicating that the co-planar orientation of the rings A and B does not match the bioactive conformation of flufenamic acid within TAS2R14.

Within the series of flufenamic acid derivatives, ligand activity was found to be highly similar to the reference agonist flufenamic acid ($E_{\text{max}} > 90$) for ligands **11–12**, **28**, and **31**. In contrast, a ceiling effect reduced E_{max} values for the derivatives **10**, **15**, **30**, and **32**. Noteworthy, the tetrazole **32** concomitantly displayed high potency and submaximal intrinsic activity (E_{max} 67). Thus, this high potency partial agonist may represent a promising first step towards the development of high affinity TAS2R14 antagonists.

In total, 12 ligands with EC₅₀ < 1 μM (23% of all < 1 μM TAS2R14 agonists, 6% of all TAS2R14 agonists) were designed and synthesized (Fig. 2), with three of them being more potent than the lead compound flufenamic acid.

Activities of the new ligands were used to refine the TAS2R14 model (Fig. 1, step 6). A wider conformational space of the flufenamic acid/TAS2R14-binding mode was explored by induced-fit docking (IFD) simulations (Schrödinger Suite 2016-2). Mutagenesis data from Nowak et al. [36] were used to narrow down to ten interpretative models. Complexes of these TAS2R14 models with flufenamic acid analogs were generated and ROC curves were calculated for each model. The model with the best ROC curve was selected as the refined model (Fig. S2), now available through BitterDB [33] and in Supporting Information (refined_model_TAS2R14.pdb).

The modified arrangement of the binding site residues in the refined model allows a better prediction of the binding affinities of newly synthesized compounds (Fig. 3). The comparison between the docking scores obtained with the

Table 1 Activity of the target compounds in a calcium-imaging assay

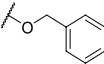
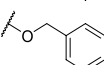
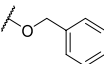
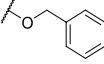
	Type I		Type II					Type III	
	Type	R ₁	R ₂	R ₃	R ₄	R ₅	Y	EC ₅₀ ± SEM (nM)	E _{max} ± SEM ^a
Flufenamic acid	I	H	COOH	H	CF ₃	H	NH	237.8 ± 12.9	100.0 ± 4.6
10	I	H	COOH	H	CH ₂ CH ₃	H	NH	993.4 ± 97.1	81.9 ± 8.3
11	I	H	COOH	H	CF ₃	CF ₃	NH	117.5 ± 5.1	107.8 ± 7.5
12	I	H	COOH	H		H	NH	846.1 ± 69.9	105.5 ± 3.8
13	I	H	COOH		H	H	NH	n.d.	10.4 ± 3.6
14	I	F	COOH		H	H	NH	n.d.	n.d.
15	I	H	COOH	H		H	NH	516.0 ± 47.8	85.2 ± 3.7
16	I	F	COOH	H		H	NH	896.0 ± 111.7	84.7 ± 2.5
17	II	H	COOH	–	–	–	NH	955.3 ± 94.0	77.5 ± 1.9
18	II	F	COOH	–	–	–	NH	n.d.	83.7 ± 3.4
20	I	H	COOH	H	CF ₃	H	NHCH ₂	n.d.	39.6 ± 3.9
22	I	H	COOH	H	CF ₃	H	O	n.d.	n.d.
28	I	H		H	CH ₂ CH ₃	H	NH	515.1 ± 52.7	94.3 ± 6.2
29	II	H		–	–	–	NH	320.5 ± 17.5	87.1 ± 6.4
30	I	H		H		H	NH	504.3 ± 20.8	80.4 ± 5.6
31	I	H		H	CF ₃	H	NH	171.5 ± 23.6	115.6 ± 4.1
32	I	H		H	CF ₃	CF ₃	NH	116.6 ± 23.6	66.7 ± 11.6
33	II	H		–	–	–	NH	n.d.	n.d.
34	I	H		H		H	NH	n.d.	n.d.
38	III	–	–	–	–	–	NH	n.d.	37.0 ± 1.4

Table 1 (continued)

Cells are colored in green when ligand potency is comparable to flufenamic acid (EC_{50} range: ~100 to 600 nM), in orange if weaker ($EC_{50} > 600$ nM), and in red if potency could not be determined
n.d. not determined
^a E_{max} values were determined by taking the averaged $\Delta F/F$ values of the concentration causing the highest signal

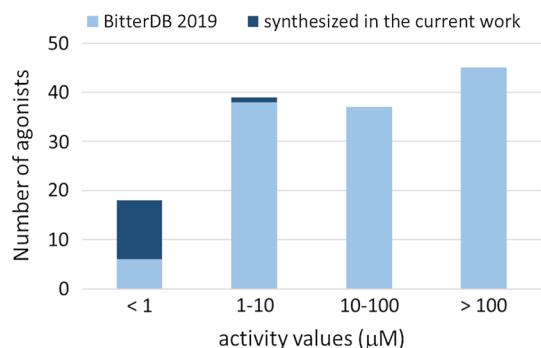


Fig. 2 Activities of old and newly synthesized agonists. Light blue bars show the distribution of TAS2R14 agonist activity values (EC_{50} or activation thresholds) as reported in the recent release of the BitterDB database [33]. The additions due to the current work are colored in dark blue

initial model and those obtained with the refined model is reported in Supplementary Table S1. While TAS2R14 initial model [36] predicted eight inactive compounds as active (orange curve, Fig. 3b), the refinement led to a different orientation of the ligand (Fig. 3a) and could discriminate between newly synthesized active and inactive compounds (ROC curve in cyan, Fig. 3b).

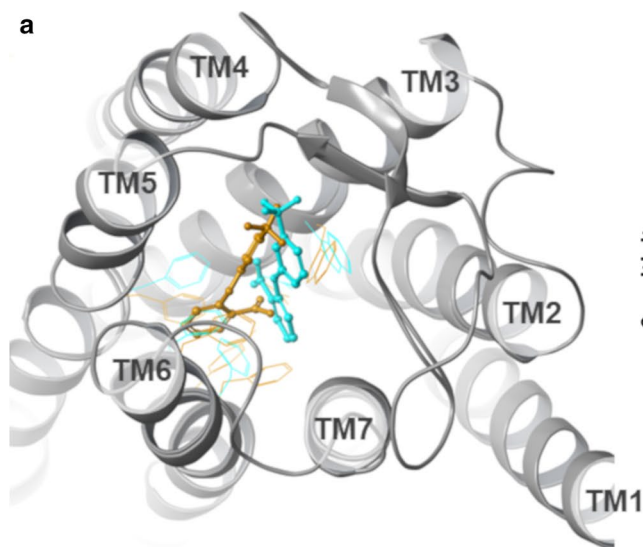
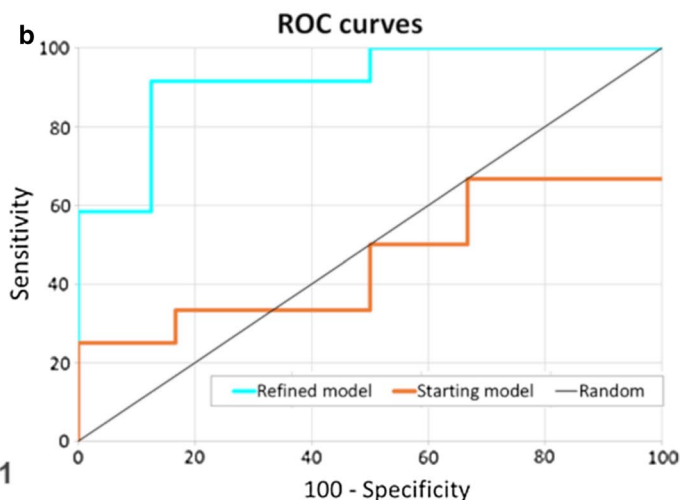


Fig. 3 a Refined flufenamic acid/TAS2R14 (in cyan) vs. initial flufenamic acid/TAS2R14 model (orange). **b** ROC curves obtained using refined TAS2R14 (in cyan) and initial TAS2R14 model [36]

As shown in Fig. 4, flufenamic acid is predicted to H bond with Asn93^{3,36} and to form hydrophobic interactions with the residues that shape the binding site: the hydrophobic three phenylalanine subpockets formed by Phe186^{5,46}, Phe243^{6,51}, and Phe247^{6,55} on one side, and Trp89^{3,32} on the other side, Ile148^{4,61} and Ile262^{7,35}. Ile148^{4,61} was suggested as a TAS2R14 point contact specific for flufenamic acid recognition also in other studies [27].

Flufenamic acid in the refined model establishes similar interactions to those observed in the initial model [36], i.e., interactions with Asn93^{3,36} and Phe247^{6,55}. However, with respect to the initial model [36], the refined model highlights the importance of flufenamic acid orientation and conformation of its aromatic rings (Fig. 4). The binding modes of all flufenamic acid derivatives to the refined TAS2R14 model are shown and described in Supplementary Figs. S5–S9.

To confirm the ligand-mediated TAS2R14 activation observed in the calcium-imaging assays, a subset of the most promising compounds was further evaluated in resonance energy transfer (FRET or BRET) second messenger-based assays for the inhibition of cAMP accumulation or the generation of IP₁ (Fig. 5, Table S2). Both assays have been successfully employed to characterize agonist-mediated receptor activation for a number of different GPCRs including mu-opioid (MOR) [19], muscarinic acetylcholine (M₂R,



(orange). Flufenamic acid, 10–12, 15–17, 28–32 were used as true positives and compounds 13, 14, 18, 20, 22, 33, 34, 38 as true negatives

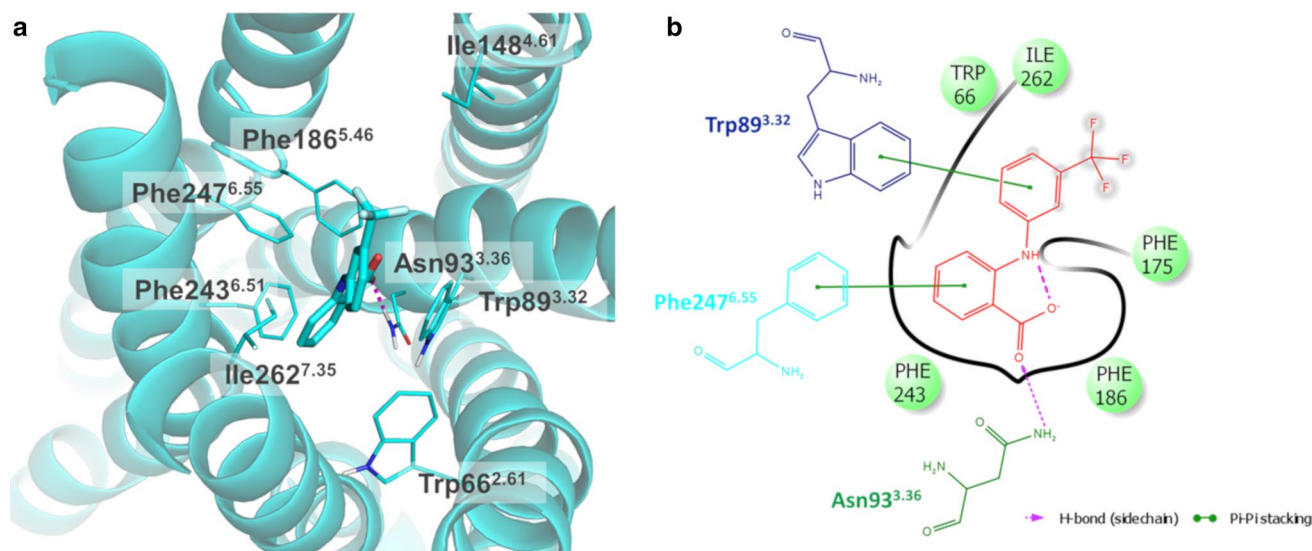
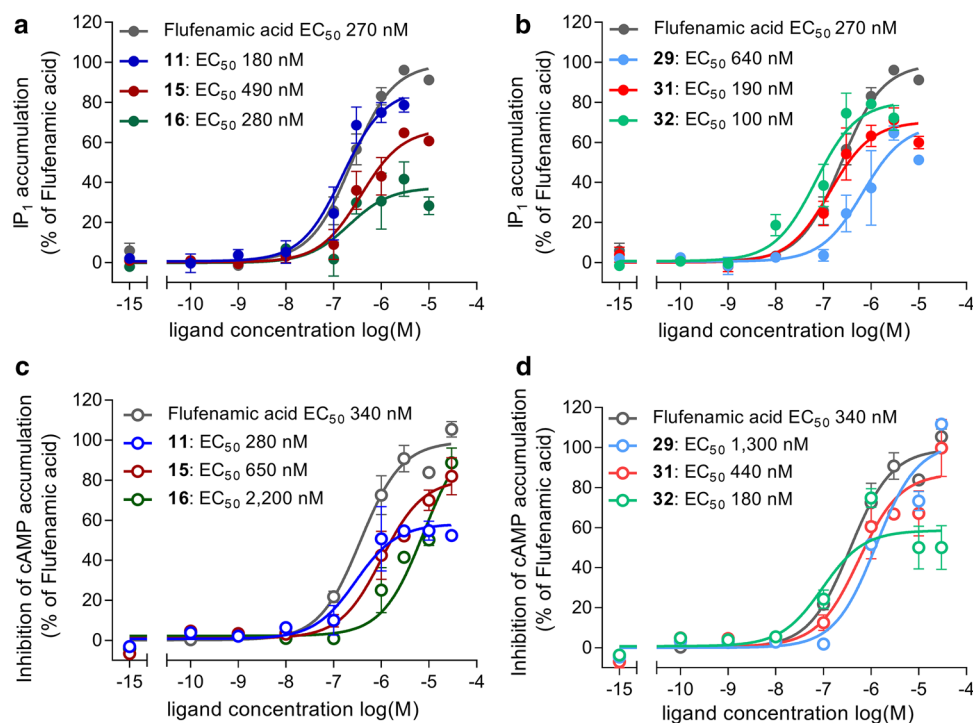


Fig. 4 **a** 3D and **b** 2D representations of refined flufenamic acid/TAS2R14 model

Fig. 5 TAS2R14 activation induced by flufenamic acid and a subset of the new ligands (**11**, **15**, **16** and **29**, **31**, **32**) can be monitored with IP-One (**a**, **b**) and cAMP (**c**, **d**) assays. Flufenamic acid shows a similar EC_{50} in both assays: 270 nM and 340 nM for IP₁ and cAMP, respectively. Both assays confirm compound **32** as high potency TAS2R14 partial agonist. Data show dose–response curves as mean \pm SEM from three independent experiments; each performed in triplicate



M_3R) [41–43], and dopamine (D_2R) [44–46] receptors. The example of agonist-mediated activation of D_2R by the native neurotransmitter dopamine, the standard reference agonist quinpirole and the approved drug aripiprazole, leading to similar efficacies and nanomolar potencies in both systems (Fig. S4), demonstrates the assays' suitability for the characterization of GPCR ligands. Similarly to the employed calcium-imaging assay, the measured accumulation of IP₁ (Fig. 5a, b) is a result of the interaction of TAS2R14

with a promiscuous G protein, $G\alpha_{q15-HA}$ [47]. In contrast, TAS2R14-mediated inhibition of cAMP formation (Fig. 5c, d) was investigated using the native alpha subunit of gustducin (GNAT3) and the cAMP-BRET sensor CAMYEL [48]. Stimulation of TAS2R14 with the reference agonist flufenamic acid resulted in overall comparable potencies (EC_{50} 270 nM and 340 nM for IP₁ and cAMP). In very good agreement with the data obtained in the initial calcium assay, ligands **11**, **31**, and **32** were identified as the most potent

flufenamic acid derivatives in the IP₁ and cAMP assays (EC₅₀ 100–190 nM for IP₁ and 180–440 nM for cAMP) and all three ligands showed substantial activity.

Importantly, tetrazole **32** showed partial agonist activity (E_{\max} 83% for IP₁; 61% for cAMP), confirming the observations from the initial calcium assay. For the two benzyloxy-substituted derivatives **15** and **16**, opposite effects were observed in the two second messenger assays. While **15** was able to elicit a response at similar ligand concentrations in both assays (EC₅₀ 490 nM/650 nM for IP₁/cAMP), **16** was roughly tenfold less potent in the cAMP assay (EC₅₀ 280 nM and 2,200 nM). In general, differences in ligand efficacy between the calcium-imaging and second messenger assays may be explained by the use of different signaling endpoints and kinetics. For instance, intracellular calcium responses are transient and tightly controlled within short times, whereas the IP-one assay detects the accumulation of IP₁, a downstream metabolite of IP₃, over a longer time period.

Discussion

Modeling, in vitro screening and medicinal chemistry were successfully combined to develop flufenamic acid derivatives as new TAS2R14 agonists. Using structure-based modeling, we have designed flufenamic acid analogs **10–18**, **20**, and **22**. Structure-based virtual screening typically provides good hit rates when crystal structures or high-resolution homology models are used [49, 50]. Given that the design of compounds was based on a very low-resolution homology model (~10% sequence identity to the template [34]), the success of our model is remarkable: 6 out of 11 molecules suggested by the docking screening were confirmed as active compounds with EC₅₀ values comparable or even superior to that of flufenamic acid.

Even though TAS2R14 is a broadly tuned receptor capable of accommodating compounds diverse in size and molecular properties [30, 34], here, we show that slight modifications in the flufenamic acid structure may drastically decrease or even abolish TAS2R14 activity. TAS2R14 responsiveness to compounds **12**, **15–17** confirms the hypothesis that TAS2R14-binding pocket can accommodate large molecules [34]. However, large side chains as ring B substituents (i.e., **12**, **15**, and **16**) are tolerated by the binding pocket if they are located in *meta*-position, but an *ortho*-substitution on ring B completely abolishes the activity. Cell-based results clearly indicate the importance of the linker region, as only the NH-linker was able to preserve the biological activity. The modeling analysis shows that these structural changes affect the relative orientation of the two aromatic rings and, consequently, the π - π -stacking interactions with the aromatic residues in the binding site. As a further validation of this interpretation, the conformationally restrained compound **38**

does not maintain the conformation of rings A and B of the flufenamic acid and has dramatically lower potency.

Using bioisosteric replacement, we could establish 5-substituted-1,2,3,4-tetrazoles as novel chemotypes for TAS2R14 ligands. The bioisosteres furnish interesting insights into the molecular determinants of ligand–receptor binding. The sulfonamides clash with adjacent residues (i.e., Fig. S8 panel 3), whereas 5-substituted tetrazoles fit well in the pocket and establish additional aromatic interactions (Fig. S9), demonstrating a well-suited replacement of the carboxylic acid. The different size of the tetrazole compared to the carboxylic acid causes a slight shift of rings A and B and, consequently, the effect of the substituents may be different. These results encourage the use of the tetrazoles, especially the novel bis-trifluoromethyl-substituted derivative **32**, as lead compounds for further structural modifications. Its high potency (EC₅₀ 100–180 nM depending on the assay) and its concomitant partial agonist activity (E_{\max} 61–83%) render **32** a promising candidate for future development of both TAS2R14 agonists and antagonists.

With the help of the derived structure–activity relationship analysis, the binding site of a low-resolution homology model was reshaped. The ROC curve obtained after model refinement shows that the refined model is able to discriminate between active and inactive compounds in this series and, therefore, is a valuable tool to guide future hit optimization processes. The refined TAS2R14 model was already successfully used to rationalize the binding mode of the bitter guaifenesin and lack of accommodation of its non-bitter prodrugs to the TAS2R14 [15]. We were able to demonstrate that structure-based ligand design, integrated with experimental data, is useful for the rationalization of ligand–receptor interactions and for the design of novel potent agonists and partial agonists. This holds even though the GPCR of interest, bitter taste receptor TAS2R14, has very low sequence similarity to available experimental structures. Our work adds to numerous virtual screening campaigns, where docking techniques successfully identified new GPCR ligands, without incorporating explicit water molecules [51, 52]. However, water molecules in the binding site may play a role in the ligand-binding mechanism [53, 54] and will be explored in future work.

Flufenamic acid, an approved non-steroidal analgesic and anti-inflammatory drug [55], is known to exert various pharmacological functions by interacting with a plethora of physiological targets including cyclooxygenases [56], ion channels [57], and androgen receptors [58]. It has been beyond the scope of this study to investigate whether the biological activity profile of flufenamic acid has been maintained in some of the synthesized derivatives. However, our proceeding studies aim to provide highly potent agonists, partial agonists, and antagonists, as tools to selectively probe and modulate the biological functions of extra-oral TAS2R14.

Ultimately, the development of high affinity ligands may contribute to the stabilization of TAS2R14, representing the initial step towards the structural determination of chemosensory receptors [59].

Methods

Virtual combinatorial library design of flufenamic acid derivatives

Commercially available building blocks for the synthesis of flufenamic acid derivatives were searched in chemical suppliers (<https://www.alfa.com/>, <http://www.acros.com/>, <https://www.sigmaaldrich.com/>). Around 500 building blocks have been found (compounds that are less suitable for synthesis were filtered out by visual inspection). CombiGlide (version 3.9, Schrödinger, LLC, New York, NY, 2015) was used to combine the scaffolds of ring A to those of ring B, resulting in a library of ~1000 molecules. Also modifications in the linker were taken into consideration. LigPrep (version 3.6, Schrödinger, LLC, New York, NY, 2015) was used to generate 3D structures and protonation states at pH 7.0 ± 0.5 of all the molecules.

Docking

Glide (version 6.9, Schrödinger, LLC, New York, NY, 2015) was used for docking the combinatorial library to the initial TAS2R14 model [36]. The grid box was centroid of docked flufenamic acid. The docking was performed with the standard precision (SP) followed by the extra-precision (XP) mode.

Model refinement

Induced-fit docking (Schrödinger Suite 2016-2 Induced Fit Docking protocol) simulations of flufenamic acid in complex with TAS2R14 were carried out to sample a wider conformational space. 701 poses were generated starting from ten structures. Ten poses were then selected according to their agreement with mutagenesis data [36]. Flufenamic acid analogs were aligned to flufenamic acid in its bound conformation (for each of the ten poses) with phase shape-based screening (version 4.7, Schrödinger, LLC, New York, NY, 2016). Complexes of the TAS2R14 models with aligned ligands were generated and refined with Glide. Predicted binding affinity was estimated with Glide XP (version 7.1, Schrödinger, LLC, New York, NY, 2016). A Glide XP score of -4.0 kcal/mol was assigned to molecules not retrieved from docking refinement. Using ligand superimposition and complex refinement to generate the complexes allowed us to analyze the effect of the

chemical modifications in the same binding mode. Using 12 actives (**flufenamic acid**, **10–12**, **15–17**, **28–32**) as true positives and 8 inactives (**13**, **14**, **18**, **20**, **22**, **33**, **34**, **38**) as true negatives, enrichment curves for all models were calculated with the enrichment calculator plugin available in the Schrödinger Suite 2016-2.

Chemistry

For the synthesis of methyl 2-(phenylamino)-benzoates **1–9**, commercially available methyl 2-bromobenzoate or methyl 2-bromo-4,5-difluorobenzoate were coupled to the respective aniline building blocks via Pd-catalyzed Buchwald–Hartwig amination [60]. Saponification of the resulting methyl 2-(phenylamino)-benzoates led to the desired carboxylic acids **10–18**. The *N*-benzyl derivative **19** was prepared by nucleophilic substitution using anthranilic acid methyl ester and 3-(trifluoromethyl)benzyl bromide. Subsequent hydrolysis with potassium hydroxide gave the carboxylic acid **20**. An Ullmann-type reaction of methyl 2-bromobenzoate and commercially available 3-trifluoromethylphenol furnished the diaryl ether **21**, which could be saponified to give the respective carboxylic acid **22** (Scheme 1).

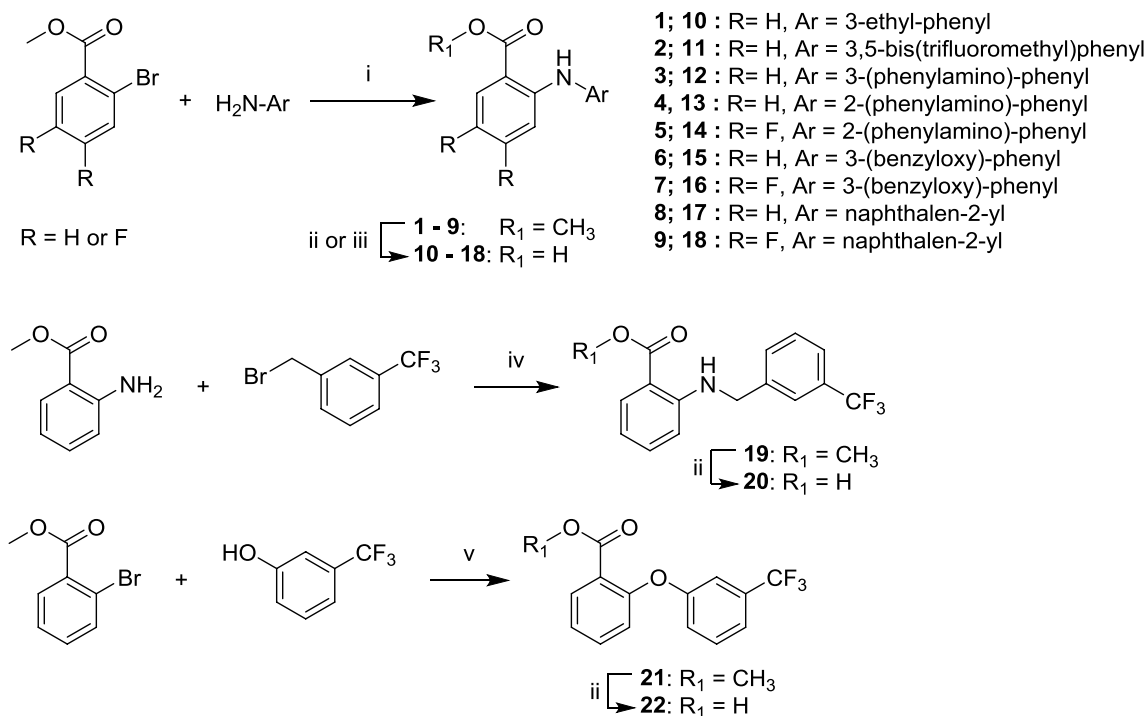
Tetrazoles **28–32** (Scheme 2) were prepared by Buchwald–Hartwig amination of 2-bromo-benzonitrile with the respective aniline building blocks followed by copper- or tin-catalyzed cycloaddition of the resulting 2-phenylamino-benzonitriles **23–27** with sodium azide. Sulfonamides **33** and **34** were synthesized in a one-step reaction using palladium(π -cinnamyl) chloride dimer, BippyPhos, and potassium phosphate.

For the synthesis of the conformationally restricted tricyclic flufenamic acid analog **38** (Scheme 2), 3-vinyl-benzoic acid **35** served as a key intermediate, which was obtained by bromination of methyl 2-bromo-3-methylbenzoate under Wohl-Ziegler conditions and subsequent substitution with triphenylphosphine. Wittig reaction of the resulting phosphonium salt with formaldehyde gave the respective olefine **35**. After re-esterification, methyl ester **36** was converted into the tricyclic derivative **37** in a Buchwald–Hartwig/Heck tandem reaction with commercially available 2-chloro-3,5-bis-trifluoromethylphenylamine. Subsequent ester hydrolysis resulted in the desired carboxylic acid **38**.

Detailed experimental procedures for the synthesis of compounds **1–38** as well as analytical data can be found in the Supporting Information.

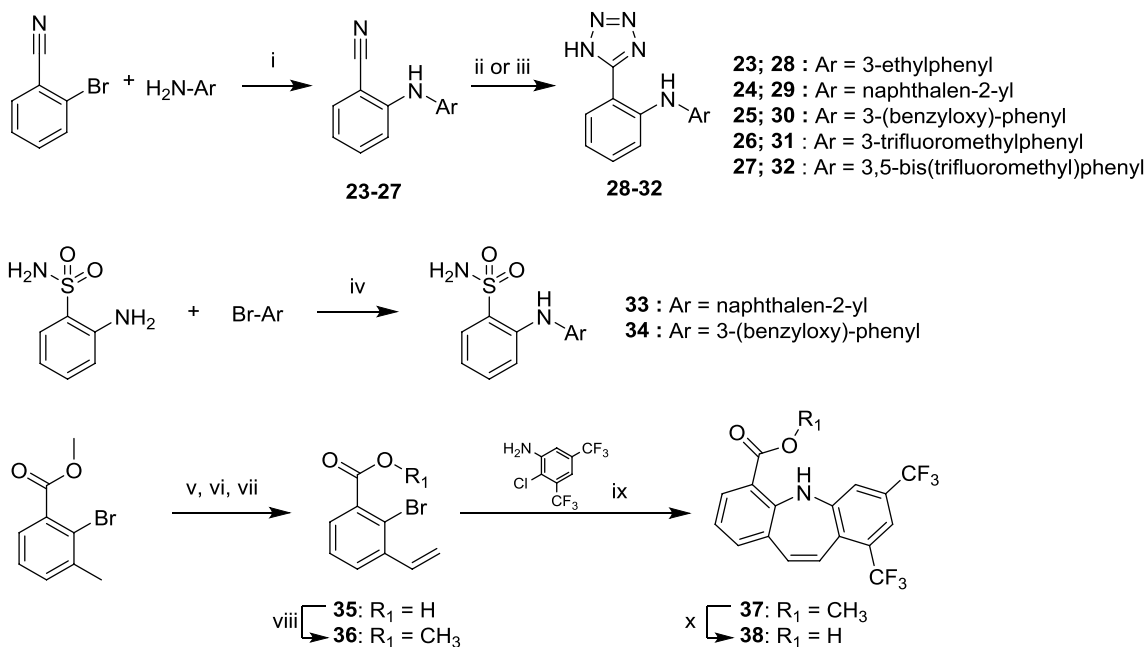
Calcium-imaging assay

HEK 293T-G α 16gust44 TAS2R14 [40] were seeded in 96-well plates and treated over night with 0.5 μ g/mL tetracycline to induce TAS2R14 expression. Cells not treated



Scheme 1 Synthesis of flufenamic acid derivatives predicted by docking: (i) Pd(OAc)₂, (±)-BINAP, Cs₂CO₃, toluene, 120 °C, 3–21 h, 28–96%; (ii) KOH, EtOH/H₂O or EtOH/H₂O/THF or MeOH/H₂O or

MeOH/THF/H₂O, reflux, 1–20 h, 42–93%; (iii) for **13**: LiOH, THF/H₂O/MeOH, 50 °C, 16 h, 77%; (iv) K₂CO₃, acetone, 65 °C, 16 h, 50%; (v) CuI, Cs₂CO₃, toluene, 125 °C, 22 h, 44%



Scheme 2 Synthesis of flufenamic acid bioisosteres **28–34** and rigidized compound **38**: (i) Pd(OAc)₂, (±)-BINAP, Cs₂CO₃, toluene, 120 °C, 3–21 h, 70–93%; (ii) for **28**: NaN₃, CuSO₄·5 H₂O, DMSO, 140 °C, 10 days, 26%; (iii) for **29–32**: NaN₃, Bu₃SnCl, TBAB, DMF, 165 °C, 23–48 h, 15–85%; (iv) [Pd(cinnamyl)Cl]₂, BippyPhos,

K₃PO₄, dioxane, 80 °C, 16 h, 33–44%; (v) *N*-bromosuccinimide, dibenzoylperoxide, CCl₄, reflux, 3 h; (vi) PPh₃, acetone, 90 °C, 6 h; (vii) CH₂O, 5 M NaOH, rt, 72 h, 24%; (viii) HCl conc., MeOH, reflux, 39 h, 94%; (x) Pd(OAc)₂, (±)-BINAP, Cs₂CO₃, toluene, 120 °C, 21 h, 4%; (x) 2 M NaOH, ethanol, 90 °C, 1 h, 81%

with tetracycline served as negative controls. Next, cells were loaded with the calcium-sensitive dye Fluo4-am in the presence of 2.5 mM probenecid. Cells were washed twice with C1-buffer (130 mM NaCl, 5 mM KCl, 10 mM Hepes, 2 mM CaCl₂, and 10 mM glucose (pH 7.4) and placed at ambient temperature in an automated fluorometric imaging plate reader (FLIPR^{tetra}, Molecular Devices). Ligands were automatically applied at different concentrations and changes in fluorescence after stimulation were monitored. For calculations of dose–response curves, the peak fluorescence responses after compound addition were corrected for background fluorescence, and baseline noise was subtracted. Dose–response curves were generated by non-linear regression (using the function $f(x) = \{ (a - d) / [1 + (x/EC_{50})^{nH}] + d \}$) with SigmaPlot software. At least three independent experiments in duplicates were performed.

IP-one assay

The measurement of TAS2R14 stimulated activation of the G protein mediated pathway was performed applying the IP-One HTRF assay (Cisbio) according to the manufacturer's protocol and in analogy to previously described procedures [41]. In brief, HEK 293T cells were grown to a confluency of approximately 80% and transiently transfected with the cDNAs of the hybrid G protein $G\alpha_{qi5-HA}$ ($G\alpha_q$ protein with the five C-terminal amino acids replaced by the corresponding sequence of $G\alpha_i$; gift from J. David Gladstone Institutes San Francisco, CA, USA) [47] and an N-terminally modified human TAS2R14 (fusion of a haemagglutinin (HA) signal followed by a Flag-tag and the first 45 amino acids of rat somatostatin receptor 3) [61] applying TransIT-293 Mirus transfection reagent (PepLab). The next day, 1.0×10^4 cells per well were seeded into black 384-well plates (Greiner Bio-One) and maintained for 24 h at 37 °C. After incubation with the test compounds dissolved in stimulation buffer at 37 °C for 150 min, the detection reagents were added (IP1-d2 conjugate and Anti-IP1 cryptate TB conjugate, each dissolved in lysis buffer), and incubation was continued at rt for 60 min. Time-resolved fluorescence resonance energy transfer was determined using a Clariostar plate reader (BMG) equipped with 620 ± 10 nm and 670 ± 10 nm filters. Dose–response curves were fitted by non-linear regression using the algorithms of PRISM 6.0 (Graphpad). Each compound was tested in triplicate in three individual experiments in comparison to the reference agonist flufenamic acid.

cAMP-BRET assay

Inhibition of forskolin stimulated cAMP accumulation mediated by TAS2R14 was measured using the biosensor

CAMYEL [48] in analogy to a previously described protocol [45]. HEK 293T cells were transiently transfected with pcDNA2L-His-CAMYEL and the modified TAS2R14 using Mirus TransIT-293 transfection reagent. 24 h post-transfection, 2.0×10^4 cells per well were seeded into white half-area 96-well plates (Greiner Bio-One). The next day, phenol red free medium was replaced by PBS and cells were serum starved for 1 h. The assay was started by adding 10 μ L coelenterazine-h (final concentration 5 μ M, Promega). After 5 min, ligands were added in PBS containing 50 μ M forskolin (final concentration 10 μ M). After additional 10 min of incubation, BRET readings were collected using a Clariostar plate reader equipped with a BRET¹ filter set. Obtained BRET ratios (emission at 535–30 nm/emission at 475–30 nm) were analyzed by non-linear regression using the algorithms of PRISM 6.0. Each compound was tested in triplicate in three individual experiments in comparison to the reference agonist flufenamic acid.

Acknowledgements This research was supported in part by the German Research Foundation Grants Gm 13/12 (to P.G. and M.Y.N.), GRK 1910 (to P.G.), and ISF 494/16 (to M.Y.N). Lady Davis Fellowship and COST-STSM-CM1207 (GLISTEN) to A.D.P. are gratefully acknowledged. M.Y.N and A.D.P. participate in Mu.Ta.Lig—COST ACTION CA15135. The authors would like to thank Catherine Delaporte for the excellent technical assistance and Tamir Dingjan for the critical reading of the manuscript.

References

- Jacobson KA (2015) New paradigms in GPCR drug discovery. *Biochem Pharmacol* 98(4):541–555
- Hauser AS, Attwood MM, Rask-Andersen M, Schiöth HB, Gloriam DE (2017) Trends in GPCR drug discovery: new agents, targets and indications. *Nat Rev Drug Discov* 16(12):829–842. <https://doi.org/10.1038/nrd.2017.178>
- Pluskal T, Weng JK (2018) Natural product modulators of human sensations and mood: molecular mechanisms and therapeutic potential. *Chem Soc Rev* 47(5):1592–1637. <https://doi.org/10.1039/c7cs00411g>
- Di Pizio A, Ben Shoshan-Galeczki Y, Hayes JE, Niv MY (2018) Bitter and sweet tasting molecules: it's complicated. *Neurosci Lett*. <https://doi.org/10.1016/j.neulet.2018.04.027>
- Wang M, Yao Y, Kuang D, Hampson DR (2006) Activation of family C G-protein-coupled receptors by the tripeptide glutathione. *J Biol Chem* 281(13):8864–8870. <https://doi.org/10.1074/jbc.M512865200>
- Di Pizio A, Niv MY (2014) Computational studies of smell and taste receptors. *Isr J Chem* 54(8–9):1205–1218. <https://doi.org/10.1002/ijch.201400027>
- Takeda S, Kadowaki S, Haga T, Takaesu H, Mitaku S (2002) Identification of G protein-coupled receptor genes from the human genome sequence. *FEBS Lett* 520(1):97–101. [https://doi.org/10.1016/S0014-5793\(02\)02775-8](https://doi.org/10.1016/S0014-5793(02)02775-8)
- Behrens M, Meyerhof W (2010) Oral and extraoral bitter taste receptors. *Results Probl Cell Differ* 52:87–99

9. Trivedi BP (2012) Neuroscience: hardwired for taste. *Nature* 486(7403):S7–S9. <https://doi.org/10.1038/486S7a>
10. Clark AA, Dotson CD, Elson AET, Voigt A, Boehm U, Meyerhof W, Steinle NI, Munger SD (2015) TAS2R bitter taste receptors regulate thyroid function. *FASEB J* 29(1):164–172. <https://doi.org/10.1096/fj.14-262246>
11. Lee R, Cohen N (2015) Taste receptors in innate immunity. *Cell Mol Life Sci* 72(2):217–236. <https://doi.org/10.1007/s00018-014-1736-7>
12. Malki A, Fiedler J, Fricke K, Ballweg I, Pfaffl MW, Krautwurst D (2015) Class I odorant receptors, TAS1R and TAS2R taste receptors, are markers for subpopulations of circulating leukocytes. *J Leukoc Biol*. <https://doi.org/10.1189/jlb.2a0714-331rr>
13. Di Pizio A, Behrens M, Krautwurst D (2019) Beyond the flavour: the potential druggability of chemosensory G protein-coupled receptors. *Int J Mol Sci*. <https://doi.org/10.3390/ijms20061402>
14. Drewnowski A, Gomez-Carneros C (2000) Bitter taste, phytonutrients, and the consumer: a review. *Am J Clin Nutr* 72(6):1424–1435
15. Thawabteh A, Lelario F, Scrano L, Bufo SA, Nowak S, Behrens M, Di Pizio A, Niv MY, Karaman R (2018) Bitterless guaifenesin prodrugs—design, synthesis, characterization, in vitro kinetics and bitterness studies. *Chem Biol Drug Des*. <https://doi.org/10.1111/cbdd.13409>
16. Lee SJ, Depoortere I, Hatt H (2019) Therapeutic potential of ectopic olfactory and taste receptors. *Nat Rev Drug Discov* 18(2):116–138. <https://doi.org/10.1038/s41573-018-0002-3>
17. Stern L, Giese N, Hackert T, Strobel O, Schirmacher P, Felix K, Gaida MM (2018) Overcoming chemoresistance in pancreatic cancer cells: role of the bitter taste receptor T2R10. *J Cancer* 9(4):711–725. <https://doi.org/10.7150/jca.21803>
18. Hilger D, Masureel M, Kobilka BK (2018) Structure and dynamics of GPCR signaling complexes. *Nat Struct Mol Biol* 25(1):4–12. <https://doi.org/10.1038/s41594-017-0011-7>
19. Manglik A, Lin H, Aryal DK, McCorvy JD, Dengler D, Corder G, Levit A, Kling RC, Bernat V, Hübner H, Huang X-P, Sassano MF, Giguère PM, Löber S, Da D, Scherrer G, Kobilka BK, Gmeiner P, Roth BL, Shoichet BK (2016) Structure-based discovery of opioid analgesics with reduced side effects. *Nature* 537(7619):185–190. <https://doi.org/10.1038/nature19112>
20. Männel B, Jaiteh M, Zeifman A, Randakova A, Möller D, Hübner H, Gmeiner P, Carlsson J (2017) Structure-guided screening for functionally selective D2 dopamine receptor ligands from a virtual chemical library. *ACS Chem Biol* 12(10):2652–2661. <https://doi.org/10.1021/acscchembio.7b00493>
21. Di Pizio A, Kruetzfeldt LM, Cheled-Shoval S, Meyerhof W, Behrens M, Niv MY (2017) Ligand binding modes from low resolution GPCR models and mutagenesis: chicken bitter taste receptor as a test-case. *Sci Rep* 7(1):8223. <https://doi.org/10.1038/s41598-017-08344-9>
22. Brockhoff A, Behrens M, Niv MY, Meyerhof W (2010) Structural requirements of bitter taste receptor activation. *Proc Natl Acad Sci USA* 107(24):11110–11115. <https://doi.org/10.1073/pnas.0913862107>
23. Born S, Levit A, Niv MY, Meyerhof W, Behrens M (2013) The human bitter taste receptor TAS2R10 is tailored to accommodate numerous diverse ligands. *J Neurosci* 33(1):201–213
24. Di Pizio A, Shy N, Behrens M, Meyerhof W, Niv MY (2018) Molecular features underlying selectivity in chicken bitter taste receptors. *Front Mol Biosci* 5:6. <https://doi.org/10.3389/fmolb.2018.00006>
25. Sandal M, Behrens M, Brockhoff A, Musiani F, Giorgetti A, Carloni P, Meyerhof W (2015) Evidence for a transient additional ligand binding site in the TAS2R46 bitter taste receptor. *J Chem Theory Comput* 11(9):4439–4449. <https://doi.org/10.1021/acs.jctc.5b00472>
26. Biarnés X, Marchiori A, Giorgetti A, Lanzara C, Gasparini P, Carloni P, Born S, Brockhoff A, Behrens M, Meyerhof W (2010) Insights into the binding of phenylthiocarbamide (PTC) agonist to its target human TAS2R38 bitter receptor. *PLoS One* 5(8):e12394. <https://doi.org/10.1371/journal.pone.0012394>
27. Jagupilli A, Singh N, De Jesus VC, Gounni MS, Dhanaraj P, Chelikani P (2018) Chemosensory bitter taste receptors (T2Rs) are activated by multiple antibiotics. *FASEB J*. <https://doi.org/10.1096/fj.201800521rr>
28. Hariri BM, McMahon DB, Chen B, Freund JR, Mansfield CJ, Doghramji LJ, Adappa ND, Palmer JN, Kennedy DW, Reed DR, Jiang P, Lee RJ (2017) Flavones modulate respiratory epithelial innate immunity: anti-inflammatory effects and activation of the T2R14 receptor. *J Biol Chem* 292(20):8484–8497
29. Gentiluomo M, Crifasi L, Luddi A, Locci D, Barale R, Piomboni P, Campa D (2017) Taste receptor polymorphisms and male infertility. *Hum Reprod* 32(11):2324–2331. <https://doi.org/10.1093/humrep/dex305>
30. Levit A, Nowak S, Peters M, Wiener A, Meyerhof W, Behrens M, Niv MY (2014) The bitter pill: clinical drugs that activate the human bitter taste receptor TAS2R14. *FASEB J* 28(3):1181–1197. <https://doi.org/10.1096/fj.13-242594>
31. Behrens M, Gu M, Fan SJ, Huang C, Meyerhof W (2018) Bitter substances from plants used in traditional Chinese medicine exert biased activation of human bitter taste receptors. *Chem Biol Drug Des* 91(2):422–433. <https://doi.org/10.1111/cbdd.13089>
32. Di Pizio A, Niv MY (2015) Promiscuity and selectivity of bitter molecules and their receptors. *Bioorg Med Chem* 23(14):4082–4091. <https://doi.org/10.1016/j.bmc.2015.04.025>
33. Dagan-Wiener A, Di Pizio A, Nissim I, Bahia MS, Dubovski N, Margulis E, Niv MY (2018) BitterDB: taste ligands and receptors database in 2019. *Nucleic Acids Res*. <https://doi.org/10.1093/nar/gky974>
34. Karaman R, Nowak S, Di Pizio A, Kitaneh H, Abu-Jaish A, Meyerhof W, Niv MY, Behrens M (2016) Probing the binding pocket of the broadly tuned human bitter taste receptor TAS2R14 by chemical modification of cognate agonists. *Chem Biol Drug Des* 88(1):66–75. <https://doi.org/10.1111/cbdd.12734>
35. Ballesteros JA, Weinstein H (1995) [19] Integrated methods for the construction of three-dimensional models and computational probing of structure-function relations in G protein-coupled receptors. *Methods Neurosci* 25(25):366–428. [https://doi.org/10.1016/s1043-9471\(05\)80049-7](https://doi.org/10.1016/s1043-9471(05)80049-7)
36. Nowak S, Di Pizio A, Levit A, Niv MY, Meyerhof W, Behrens M (2018) Reengineering the ligand sensitivity of the broadly tuned human bitter taste receptor TAS2R14. *Biochim Biophys Acta* 1862(10):2162–2173. <https://doi.org/10.1016/j.bbagen.2018.07.009>
37. Lassalas P, Gay B, Lasfargeas C, James MJ, Tran V, Vijayendran KG, Brunden KR, Kozlowski MC, Thomas CJ, Smith AB 3rd, Huryn DM, Ballatore C (2016) Structure property relationships of carboxylic acid isosteres. *J Med Chem* 59(7):3183–3203
38. Fang Z, Yn Song, Zhan P, Zhang Q, Liu X (2014) Conformational restriction: an effective tactic in ‘follow-on’-based drug discovery. *Future Med Chem* 6(8):885–901. <https://doi.org/10.4155/fmc.14.50>
39. Ueda T, Ugawa S, Yamamura H, Imaizumi Y, Shimada S (2003) Functional interaction between T2R taste receptors and G-protein α subunits expressed in taste receptor cells. *J Neurosci* 23(19):7376–7380. <https://doi.org/10.1523/JNEUROSCI.23-19-07376.2003>
40. Behrens M, Blank K, Meyerhof W (2017) Blends of non-caloric sweeteners saccharin and cyclamate show reduced off-taste due

- to TAS2R bitter receptor inhibition. *Cell Chem Biol* 24(10):1199. <https://doi.org/10.1016/j.chembiol.2017.08.004>
41. Fish I, Stöbel A, Eitel K, Valant C, Albold S, Hübner H, Möller D, Clark MJ, Sunahara RK, Christopoulos A, Shoichet BK, Gmeiner P (2017) Structure-based design and discovery of new M2 receptor agonists. *J Med Chem* 60(22):9239–9250. <https://doi.org/10.1021/acs.jmedchem.7b01113>
 42. Liu H, Hofmann J, Fish I, Schaake B, Eitel K, Bartuschat A, Kaindl J, Rampp H, Banerjee A, Hübner H, Clark MJ, Vincent SG, Fisher JT, Heinrich MR, Hirata K, Liu X, Sunahara RK, Shoichet BK, Kobilka BK, Gmeiner P (2018) Structure-guided development of selective M3 muscarinic acetylcholine receptor antagonists. *Proc Natl Acad Sci* 115(47):12046–12050
 43. Pegoli A, She X, Wifling D, Hübner H, Bernhardt G, Gmeiner P, Keller M (2017) Radiolabeled dibenzodiazepinone-type antagonists give evidence of dualsteric binding at the M2 muscarinic acetylcholine receptor. *J Med Chem* 60(8):3314–3334. <https://doi.org/10.1021/acs.jmedchem.6b01892>
 44. Lachmann D, Studte C, Männel B, Hübner H, Gmeiner P, König B (2017) Photochromic dopamine receptor ligands based on dithienylethenes and fulgides. *Chemistry* 23(54):13423–13434. <https://doi.org/10.1002/chem.201702147>
 45. Sommer T, Hübner H, El Kerdawy A, Gmeiner P, Pischetsrieder M, Clark T (2017) Identification of the beer component horde-nine as food-derived dopamine D2 receptor agonist by virtual screening a 3D compound database. *Sci Rep* 7:44201. <https://doi.org/10.1038/srep44201>
 46. Hübner H, Schellhorn T, Gienger M, Schaab C, Kaindl J, Leeb L, Clark T, Möller D, Gmeiner P (2016) Structure-guided development of heterodimer-selective GPCR ligands. *Nat Commun* 7:12298. <https://doi.org/10.1038/ncomms12298>
 47. Conklin BR, Farfel Z, Lustig KD, Julius D, Bourne HR (1993) Substitution of three amino acids switches receptor specificity of Gq alpha to that of Gi alpha. *Nature* 363(6426):274–276. <https://doi.org/10.1038/363274a0>
 48. Jiang LI, Collins J, Davis R, Lin KM, DeCamp D, Roach T, Hsueh R, Rebres RA, Ross EM, Taussig R, Fraser I, Sternweis PC (2007) Use of a cAMP BRET sensor to characterize a novel regulation of cAMP by the sphingosine 1-phosphate/G(13) pathway. *J Biol Chem* 282(14):10576–10584. <https://doi.org/10.1074/jbc.M609695200>
 49. Du H, Brender JR, Zhang J, Zhang Y (2015) Protein structure prediction provides comparable performance to crystallographic structures in docking-based virtual screening. *Methods* 71:77–84. <https://doi.org/10.1016/j.ymeth.2014.08.017>
 50. Congreve M, Oswald C, Marshall FH (2017) Applying structure-based drug design approaches to allosteric modulators of GPCRs. *Trends Pharmacol Sci* 38(9):837–847. <https://doi.org/10.1016/j.tips.2017.05.010>
 51. Lyu J, Wang S, Balias TE, Singh I, Levit A, Moroz YS, O'Meara MJ, Che T, Algae E, Tolmacheva K, Tolmachev AA, Shoichet BK, Roth BL, Irwin JJ (2019) Ultra-large library docking for discovering new chemotypes. *Nature* 566(7743):224. <https://doi.org/10.1038/s41586-019-0917-9>
 52. Roth BL, Irwin JJ, Shoichet BK (2017) Discovery of new GPCR ligands to illuminate new biology. *Nat Chem Biol* 13(11):1143–1151. <https://doi.org/10.1038/nchembio.2490>
 53. Jaggupilli A, Howard R, Upadhyaya JD, Bhullar RP, Chelikani P (2016) Bitter taste receptors: novel insights into the biochemistry and pharmacology. *Int J Biochem Cell B* 77:184–196. <https://doi.org/10.1016/j.biocel.2016.03.005>
 54. Venkatakrisnan AJ, Ma AK, Fonseca R, Latorraca NR, Kelly B, Betz RM, Asawa C, Kobilka BK, Dror RO (2019) Diverse GPCRs exhibit conserved water networks for stabilization and activation. *Proc Natl Acad Sci USA* 116(8):3288–3293. <https://doi.org/10.1073/pnas.1809251116>
 55. Rajan KT, Hill AG, Barr A, Whitwell E (1967) Flufenamic acid in rheumatoid arthritis. *Ann Rheum Dis* 26(1):43
 56. Ouellet M, Falgueyret J-P, Percival MD (2004) Detergents profoundly affect inhibitor potencies against both cyclo-oxygenase isoforms. *Biochem J* 377(3):675
 57. Guinamard R, Simard C, Del Negro C (2013) Flufenamic acid as an ion channel modulator. *Pharmacol Ther* 138(2):272–284. <https://doi.org/10.1016/j.pharmthera.2013.01.012>
 58. Féau C, Arnold LA, Kosinski A, Zhu F, Connelly M, Guy RK (2009) Novel flufenamic acid analogues as inhibitors of androgen receptor mediated transcription. *ACS Chem Biol* 4(10):834–843. <https://doi.org/10.1021/cb900143a>
 59. Zhang X, Stevens RC, Xu F (2015) The importance of ligands for G protein-coupled receptor stability. *Trends Biochem Sci* 40(2):79–87. <https://doi.org/10.1016/j.tibs.2014.12.005>
 60. Adeniji AO, Twenter BM, Byrns MC, Jin Y, Chen M, Winkler JD, Penning TM (2012) Development of potent and selective inhibitors of aldo-keto reductase 1C3 (type 5 17beta-hydroxysteroid dehydrogenase) based on *N*-phenyl-aminobenzoates and their structure-activity relationships. *J Med Chem* 55(5):2311–2323. <https://doi.org/10.1021/jm201547v>
 61. Behrens M, Brockhoff A, Kuhn C, Bufer B, Winnig M, Meyerhof W (2004) The human taste receptor hTAS2R14 responds to a variety of different bitter compounds. *Biochem Biophys Res Commun* 319(2):479–485. <https://doi.org/10.1016/j.bbrc.2004.05.019>

Publisher's Note Springer Nature remains neutral with regard to jurisdictional claims in published maps and institutional affiliations.